STRUCTURAL BIOLOGY

Structural basis of G_s and G_i recognition by the human glucagon receptor

Anna Qiao[1,2,3]*, Shuo Han[1,2]*, Xinmei Li[3,4]*, Zhixin Li[5]*, Peishen Zhao[6]*, Antao Dai[1,7], Rulve Chang[5], Linhua Tai[3,4], Qiuxiang Tan[1,2], Xiaojing Chu[1,2], Limin Ma[1,2], Thor Seneca Thorsen[8], Steffen Reedtz-Runge[8], Dehua Yang[1,7], Ming-Wei Wang[1,3,5,7,9], Patrick M. Sexton[5,6], Denise Wootten[5,6]†, Fei Sun[3,4,10]†, Qiang Zhao[2,3,11]†, Beili Wu[1,3,9,11]†

Class B G protein–coupled receptors, an important class of therapeutic targets, signal mainly through the G_s class of heterotrimeric G proteins, although they do display some promiscuity in G protein binding. Using cryo–electron microscopy, we determined the structures of the human glucagon receptor (GCGR) bound to glucagon and distinct classes of heterotrimeric G proteins, G_s or G_{i1}. These two structures adopt a similar open binding cavity to accommodate G_s and G_{i1}. The G_s binding selectivity of GCGR is explained by a larger interaction interface, but there are specific interactions that affect G_i more than G_s binding. Conformational differences in the receptor intracellular loops were found to be key selectivity determinants. These distinctions in transducer engagement were supported by mutagenesis and functional studies.

Upon binding to extracellular agonists, G protein–coupled receptors (GPCRs) stimulate various signaling pathways by recruiting different heterotrimeric G proteins ($G\alpha\beta\gamma$) to mediate a wide variety of physiological functions (*1*). The selective coupling between a GPCR and specific G proteins is critical for the physiological action of the receptor in response to its endogenous ligands and therapeutic agents. However, the molecular details that define how an individual GPCR recognizes different G protein subtypes remain elusive. Class B GPCRs canonically exert their physiological actions by producing cyclic adenosine monophosphate (cAMP) through G_s signaling; however, they also couple to other G proteins such as $G_{i/o}$ and $G_{q/11}$, leading to diverse cellular responses (*2*–*7*). Recently, structures of four class B GPCRs bound to G_s were determined by single-particle cryo–electron microscopy (cryo-EM) (*8*–*12*), but the lack of structures with other G proteins limits our understanding of molecular mechanisms driving pleiotropic coupling and biased agonism that are important considerations for drug development.

The human glucagon receptor (GCGR), a member of the class B GPCR family, is critical to glucose homeostasis by triggering the release of glucose from the liver (*13*). Previous studies in native tissues and recombinant cell lines using different assays demonstrated that glucagon, in addition to promoting cAMP formation, activates other downstream effectors that are pertussis toxin–sensitive or phospholipase C–dependent, revealing $G_{i/o}$ and $G_{q/11}$ signaling of GCGR (*14*–*18*). Selective activation of G_i in mouse hepatocytes in vivo was also reported to cause a pronounced increase in glucose production and severely impaired glucose homeostasis (*19*), which suggest that other subtypes of hepatic G proteins contribute to glucose regulation. There is interest in GCGR as a therapeutic target for type 2 diabetes and obesity (*20*). However, glucagon biology is complex; it can increase energy expenditure but high levels are diabetogenic, and drugs that selectively target GCGR are not currently available for treatment of diabetes and obesity. To better elucidate the molecular mechanisms underlying the G protein selectivity of GCGR, we determined the cryo-EM structures of GCGR in complex with its cognate ligand glucagon and heterotrimeric G_s or G_{i1} protein. These structures, combined with pharmacological data, provide important insights into GCGR activation, pleiotropic coupling, and G protein specificity.

Overall structures of G_s- and G_{i1}-bound GCGR

To obtain the GCGR-G_s complex, we replaced the native signal peptide of GCGR with that of hemagglutinin and removed 45 residues at the receptor C terminus (construct 1). Functional assays show that these modifications had little effect on glucagon binding and G_s and G_i activation of the receptor (fig. S1, A to C). To solve the GCGR-G_i structure, we further introduced three mutations—E126R, $T200^{2.73b}$W, and $A366^{6.57b}$M (construct 2)—to increase glucagon binding affinity and glucagon potency in G protein activation (fig. S1, A to C). [Superscripts refer to the Wootten numbering system for class B GPCRs, a modified form of the Ballesteros-Weinstein system for class A GPCRs (*21*).] These mutations may stabilize the receptor in a conformation favorable for G_i coupling and thus improve the stability and yield of the glucagon-GCGR-G_{i1} complex (fig. S1D). The glucagon-GCGR-G_s and glucagon-GCGR-G_{i1} structures were determined by cryo-EM single-particle analysis with an overall resolution of 3.7 Å and 3.9 Å, respectively (Fig. 1, figs. S2 and S3, and table S1) (*22*).

In the glucagon-GCGR-G_s and glucagon-GCGR-G_{i1} complexes, the glucagon binds at a site similar to that of the peptide in a structure of GCGR bound to the partial agonist NNC1702 (*23*) (fig. S4A). Structural differences in the peptide binding site between these structures occur in the region of the second and third extracellular loops (ECL2 and ECL3) and their connected transmembrane helices IV, V, VI, and VII (fig. S5, A to C). These conformational rearrangements may initiate the conformational changes of the receptor transmembrane helical bundle on the extracellular side that accompany receptor activation and transducer coupling in both the G_s- and G_{i1}-bound complexes (*22*).

A common G protein–binding pocket for G_s and G_{i1}

The intracellular half of the receptor in the glucagon-GCGR–G protein structures exhibits conformational changes relative to the inactive GCGR structure. The intracellular tip of helix VI moves away from the central axis of the helical bundle by ~19 Å (fig. S5D). Furthermore, to create a binding cavity for the G proteins, the intracellular ends of helices V and VII move outward by 8 Å and 2 Å, respectively. These conformational transitions are conserved regardless of the class of G protein that is coupled, generating a common binding pocket for both G_s and G_i (Fig. 2A).

In contrast to the common binding pocket of GCGR for G_s and G_{i1}, structures of class A GPCR–G protein complexes revealed differential positioning of helix VI (Fig. 2B), leading to proposals that the positional difference of helix VI is a major determinant for the coupling

[1]CAS Key Laboratory of Receptor Research, Shanghai Institute of Materia Medica, Chinese Academy of Sciences, Shanghai 201203, China. [2]State Key Laboratory of Drug Research, Shanghai Institute of Materia Medica, Chinese Academy of Sciences, Shanghai 201203, China. [3]University of Chinese Academy of Sciences, Beijing 100049, China. [4]National Laboratory of Biomacromolecules, National Center of Protein Science–Beijing, CAS Center for Excellence in Biomacromolecules, Institute of Biophysics, Chinese Academy of Sciences, Beijing 100101, China. [5]School of Pharmacy, Fudan University, Shanghai 201203, China. [6]Drug Discovery Biology and Department of Pharmacology, Monash Institute of Pharmaceutical Sciences, Monash University, Parkville, Victoria 3052, Australia. [7]National Center for Drug Screening, Shanghai Institute of Materia Medica, Chinese Academy of Sciences, Shanghai 201203, China. [8]Novo Nordisk A/S, Måløv 2760, Denmark. [9]School of Life Science and Technology, ShanghaiTech University, Shanghai 201210, China. [10]Center for Biological Imaging, Institute of Biophysics, Chinese Academy of Sciences, Beijing 100101, China. [11]CAS Center for Excellence in Biomacromolecules, Chinese Academy of Sciences, Beijing 100101, China.
*These authors contributed equally to this work.
†Corresponding author. Email: denise.wootten@monash.edu (D.W.); feisun@ibp.ac.cn (F.S.); zhaoq@simm.ac.cn (Q.Z.); beiliwu@simm.ac.cn (B.W.)

specificity of G_s and $G_{i/o}$ in GPCRs (*24*–*30*). The displacement of the intracellular tip of helix VI in the glucagon-GCGR–G protein structures is larger than in any class A GCGR–G protein structures but is more similar to the G_s-bound structures (Fig. 2D and fig. S6) (*22*). The C-terminal α5 helix of Gα subunits plays a key role in coupling selectivity (*31*, *32*). The amino acid sequence of the α5 helix in $G\alpha_s$ and $G\alpha_i$ differs at positions G.H5.23 and G.H5.24 [common Gα numbering system (*33*)] ($G\alpha_s$, $Y^{G.H5.23}$ and $E^{G.H5.24}$; $G\alpha_{i/o}$, $C^{G.H5.23}$ and $G^{G.H5.24}$). The bulkier residues in $G\alpha_s$ require a larger pocket than $G\alpha_i$ to accommodate packing of their side chains (Fig. 2, E and F). Accordingly, it was hypothesized that G_s and $G_{i/o}$ binding to GPCRs requires a different opening size of the intracellular binding cavity (*28*). This hypothesis was supported by molecular dynamics simulation studies on the β_2 adrenergic receptor (β_2AR) in complex with C-terminal peptides derived from $G\alpha_s$ or $G\alpha_i$ (*34*).

Contrary to this hypothesis, the two GCGR–G protein structures as well as other G_s-bound class B GPCR structures (*8*–*12*) display a similar outward shift of helix VI, forming a common binding cavity for recognition of both G_s and G_i, where the backbone conformations overlay for both the receptor and the far C terminus of the Gα α5 helix (Fig. 2, A and C, and fig. S4B). However, although GCGR couples to both G proteins through this common pocket, it does so with differing efficiencies (fig. S1, A and B, and fig. S7). The measured interaction interface formed between the α5 C terminus (residues G.H5.16 to G.H5.26) and GCGR is larger for $G\alpha_s$ (802 Å^2) than for $G\alpha_i$ (551 Å^2). Therefore, preferential coupling to G_s can be explained by the open G protein–binding pocket (relative to the class A GPCR–$G_{i/o}$ structures) that is required to accommodate canonical binding to the bulkier α5 helix in G_s, but may still allow interaction with the less bulky G_i α5 helix (Fig. 2, G and H, and fig. S7). This concept likely extends to other GPCRs where the size of the G protein–binding pocket in the receptor core may reflect the receptor's ability to couple to multiple G proteins—a theory that is consistent with recent studies where receptors that canonically couple to G_s (and $G_{q,11,12,13}$) are generally more promiscuous than those that are classified as G_i-coupled (*31*).

Intracellular loops mediate G protein recognition and specificity

Although the α5 helix of Gα proteins is a key contributor to G protein selectivity, interactions with additional domains of the G protein also contribute to specificity (*31*). The interaction surface between GCGR and the α5 C terminus is larger for $G\alpha_s$ than for $G\alpha_i$; however, this surface only forms 60% of the interaction surface for $G\alpha_s$ (total interface 1276 Å^2, 1418 Å^2 including Gβ interactions), whereas it contributes 80% of the interaction surface for $G\alpha_i$ (total interface 687 Å^2, 863 Å^2 including Gβ interactions). Combined with G protein activation and signaling assays, the G_s- and G_{i1}-bound GCGR structures suggest that the intracellular loops of the receptor play critical roles in G protein engagement and specificity.

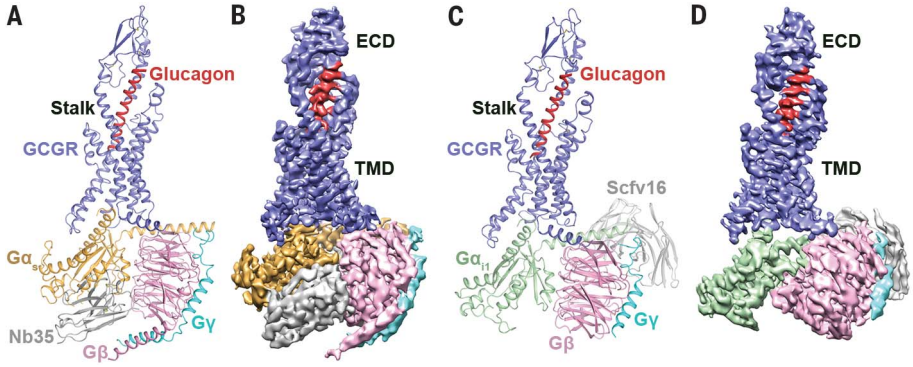

Fig. 1. Overall architectures of glucagon-GCGR–G protein complexes. (**A**) Cryo-EM structure of the glucagon-GCGR-G_s-Nb35 complex. Nb35 is a nanobody that stabilizes the interface between the $G\alpha_s$ subunit and Gβ subunit. The structure is shown in cartoon representation. GCGR, glucagon, $G\alpha_s$, Gβ, Gγ, and Nb35 are colored blue, red, gold, pink, cyan, and gray, respectively. The disulfide bonds are shown as yellow sticks. (**B**) Cryo-EM map of the glucagon-GCGR-G_S-Nb35 complex, colored according to chains. ECD, extracellular domain; TMD, transmembrane domain. (**C**) Cryo-EM structure of the glucagon-GCGR-G_{i1}-Scfv16 complex. Scfv16, the single-chain variable fragment of mAb16, stabilizes the GPCR-G_i complex by recognizing an epitope composed of the αN helix of $G\alpha_{i1}$ and the Gβ subunit. $G\alpha_{i1}$ is colored green; Scfv16 is in gray. (**D**) Cryo-EM map of the glucagon-GCGR-G_{i1}-Scfv16 complex, colored according to chains.

Comparison of the two glucagon-GCGR–G protein structures revealed a difference in the position of the Gα αN helix relative to the receptor (Fig. 3A). This N-terminal helix shifts toward the receptor in the G_{i1}-bound structure compared to that in the G_s-bound structure. This movement, along with the substitution of $A39^{G.hns1.3}$ ($G\alpha_s$) with $R32^{G.hns1.3}$ ($G\alpha_i$) at the interaction interface, is associated with a difference in the conformation of the second intracellular loop (ICL2) that alters the αN-ICL2 interface (Fig. 3A and fig. S7, F and L). In the G_s-bound structure, ICL2 forms extensive interactions with the αN helix, with A256, T257, L258, and E260 forming interactions in the binding groove between the αN helix and the β1 strand and α5 helix of $G\alpha_s$ (Fig. 3B). In contrast, when bound to G_{i1}, ICL2 adopts a position farther away from the G protein and makes only limited contact with $R32^{G.hns1.3}$ in the αN helix of $G\alpha_i$ (Fig. 3C). To investigate the role of ICL2 in activating different G protein subtypes, we assessed glucagon-induced G_s and G_{i1} activation by the wild-type and mutant GCGRs using NanoLuc Binary Technology (NanoBiT) (*35*), which measures the proximal interaction between the α and γ subunits of the G protein. In agreement with the conformational difference of ICL2, mutations L258A and E260A decreased the half-maximal effective concentration (EC_{50}) of glucagon-induced G_s activation by factors of 29 and 16, respectively, whereas they showed a much less pronounced effect on G_i activation (factor of 6 to 8 reduction of EC_{50}) (Fig. 3, F and G; fig. S8, A and D; and table S2). In all previously published GPCR–G protein structures, where the receptors couple to their cognate G protein or a noncognate G protein with comparably high affinity (NTSR1) (*36*), ICL2 forms extensive interactions with the Gα subunit. By contrast, the limited contact between ICL2 and $G\alpha_i$ observed in the G_{i1}-bound GCGR structure most likely contributes to the lower potencies of glucagon in stimulating G_i activation and signaling when compared to G_s. The above data indicate that ICL2 is crucial for the G protein specificity of GCGR.

In contrast to the importance of ICL2 in G_s coupling, other intracellular regions behave as selective determinants for G_i binding. The NanoBiT assay showed that the alanine replacement of the residue $F263^{4.41b}$ at the intracellular end of helix IV, which potentially makes contacts with the $G\alpha_i$ αN helix due to the upward shift of this N-terminal helix in G_{i1} relative to that in G_s (Fig. 3, B and C), displayed a notable loss of G_{i1} activation but a wild-type level of G_s activation (Fig. 3, F and G; fig. S8, A and D; and table S2). In association with the movement of the αN helix, the linker region between the α4 helix and β6 strand of the $G\alpha_i$ subunit approaches the third intracellular loop (ICL3) of GCGR in the glucagon-GCGR-G_{i1} complex (Fig. 3D). This was reflected by a notable decrease of glucagon potency in G_{i1} activation for the GCGR mutant H339A, which only slightly alters G_s activation (factor of 3 reduction of EC_{50}) (Fig. 3, F and G; fig. S8, A and D; and table S2). Furthermore, accompanying the positional difference of $G\alpha_i$, the Gβ and Gγ subunits shift closer to the receptor in the glucagon-GCGR-G_{i1} structure relative to the G_s-bound structure,

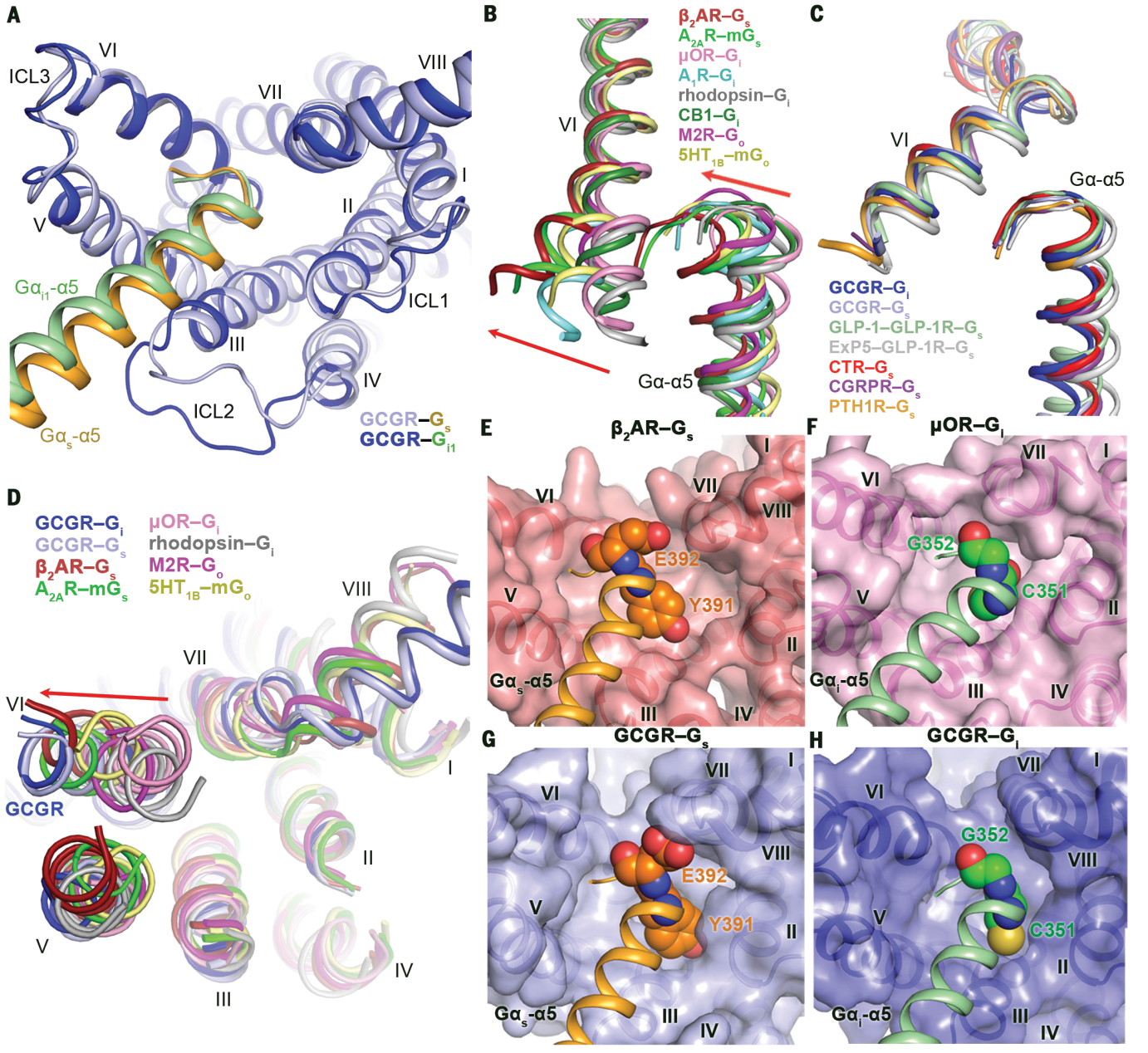

Fig. 2. Structural comparison of G protein–bound GPCR structures. (**A**) Comparison of the transmembrane helical bundle conformation and the position of Gα α5 helix C terminus in the G protein–bound GCGR structures. The glucagon-GCGR-G_s and glucagon-GCGR-G_{i1} structures are shown in cartoon representation in an intracellular view. The G_s-bound structure is colored light blue (GCGR) and gold ($G\alpha_s$); the G_{i1}-bound structure is colored dark blue (GCGR) and green ($G\alpha_{i1}$). (**B**) Comparison of the positions of helix VI and the C terminus of Gα α5 helix in the G_s- and $G_{i/o}$-bound class A GPCR structures. The structures of β_2AR-G_s, A_{2A}R–mini-G_s (mG_s), μOR-G_i, A_1R-G_i, rhodopsin-G_i, CB1-G_i, M2R-G_o, and $5HT_{1B}$–mini-G_o (mG_o) (PDB IDs: 3SN6, 6GDG, 6DDE, 6D9H, 6CMO, 6N4B, 6OIK, and 6G79) are colored dark red, green, pink, cyan, gray, dark green, magenta, and yellow, respectively. Only helix VI of the receptors and Gα α5 helix are shown for clarity. The red arrows indicate the outward tilts of helix VI and the relative shift of the C terminus of α5 helix. (**C**) Comparison of the positions of helix VI and the C terminus of Gα α5 helix in the G protein–bound class B GPCR structures. The structures of glucagon-GCGR-G_{i1} and glucagon-GCGR-G_s and the structures of GLP-1–GLP-1R–G_s, ExP5–GLP-1R–G_s, CTR-G_s, CGRPR-G_s, and PTH1R-G_s (PDB IDs: 5VAI, 6B3J, 5UZ7, 6E3Y, and 6NBF) are colored dark blue, light blue, light green, light gray, red, purple, and orange, respectively. Only helix VI of the receptors and Gα α5 helix are shown for clarity. (**D**) Comparison of the receptor helical bundles in the G protein–bound GCGR structures and class A GPCR–G protein structures in an intracellular view. The structures of glucagon-GCGR-G_{i1}, glucagon-GCGR-G_s, β_2AR-G_s, A_{2A}R-mG_s, μOR-G_i, rhodopsin-G_i, M2R-G_o, and $5HT_{1B}$-mG_o are colored dark blue, light blue, dark red, green, pink, gray, magenta, and yellow, respectively. Only the receptors in the structures are shown. The red arrow indicates the larger outward displacement of the intracellular tip of helix VI in GCGR compared to that in the G protein–bound class A GPCR structures. (**E** to **H**) Binding pocket for the Gα-α5 C terminus. (E) β_2AR-G_s; (F) μOR-G_i; (G) GCGR-G_s; (H) GCGR-G_{i1}. The Gα residues at positions G.H5.23 and G.H5.24 are shown as spheres. The α5 helices in $G\alpha_s$ and $G\alpha_i$ are colored gold and green, respectively. The receptors are shown in cartoon and surface representations in an intracellular view. Amino acid abbreviations here or elsewhere: A, Ala; C, Cys; D, Asp; E, Glu; F, Phe; G, Gly; H, His; I, Ile; K, Lys; L, Leu; N, Asn; Q, Gln; R, Arg; T, Thr; V, Val; W, Trp; Y, Tyr.

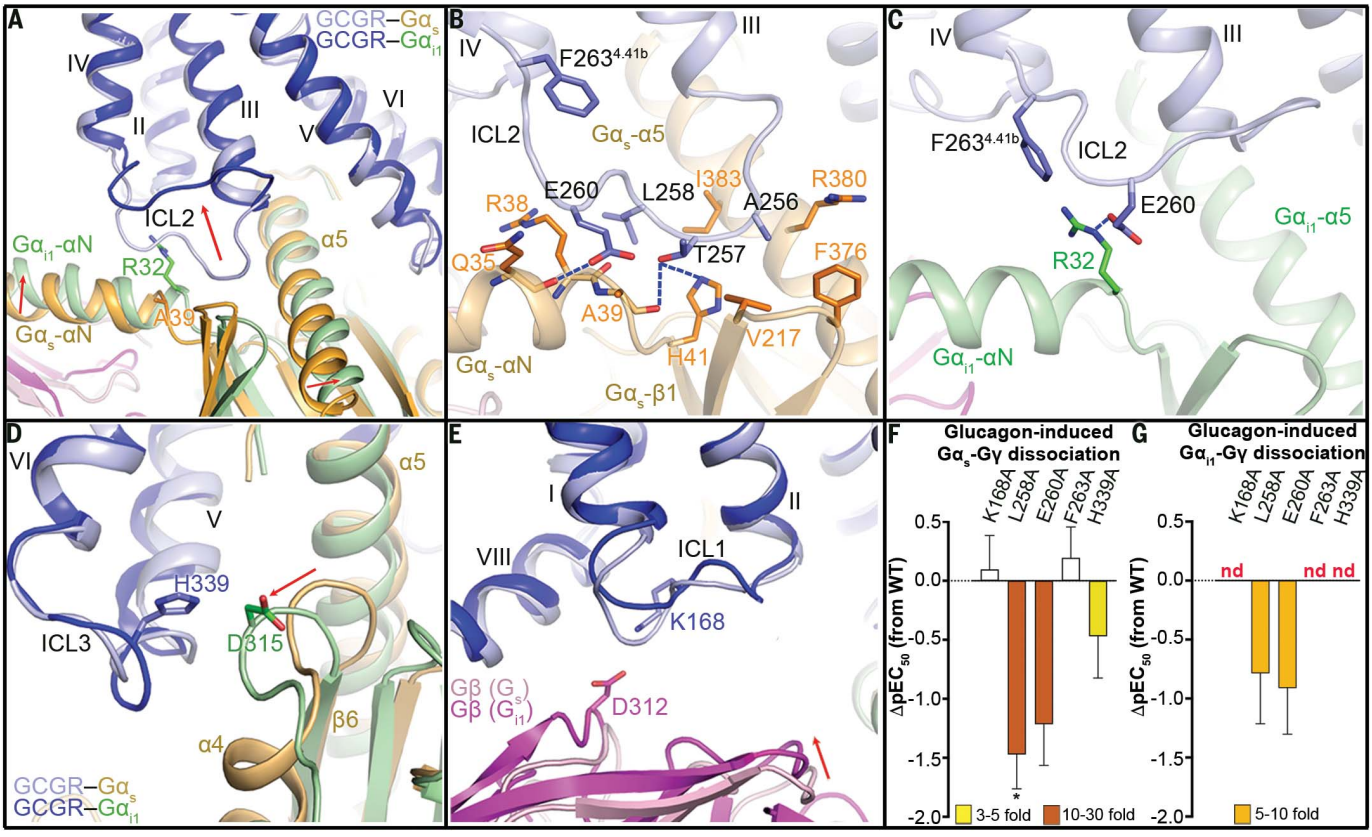

Fig. 3. G protein–binding interface mediated by GCGR intracellular loops. (**A**) Comparison of ICL2 conformation in the glucagon-GCGR-G_s and glucagon-GCGR-G_{i1} structures. The glucagon-GCGR-G_s structure is colored light blue (GCGR) and gold ($G\alpha_s$); the glucagon-GCGR-G_{i1} structure is colored dark blue (GCGR) and green ($G\alpha_{i1}$). The $G\alpha_s$ residue $A39^{G.hns1.3}$ and the $G\alpha_i$ residue $R32^{G.hns1.3}$ are shown as sticks. The red arrows indicate the movements of GCGR ICL2, $G\alpha$ α5 helix N terminus, and αN helix in the G_{i1}-bound structure relative to the G_s-bound structure. (**B**) Interactions between ICL2 and $G\alpha_s$. The residues involved in interactions are shown as sticks and are colored blue (GCGR) and orange ($G\alpha_s$). Polar interactions are shown as blue dashed lines. (**C**) Interactions between ICL2 and $G\alpha_{i1}$. The residues involved in interactions are shown as sticks and are colored blue (GCGR) and green ($G\alpha_{i1}$). (**D**) Conformational difference of the linker between the α4 helix and β6 strand in Gα. The GCGR ICL3 residue H339 and the $G\alpha_i$ residue D315 that form a contact in the glucagon-GCGR-G_{i1} structure are shown as sticks. The red arrow indicates the movement of the α4-β6 linker in the G_{i1}-bound structure relative to the G_s-bound structure. (**E**) Conformational difference of Gβ. The Gβ subunits in the two structures are colored pink (G_s) and magenta (G_{i1}). The GCGR ICL1 residue K168 and the Gβ residue D312 that form a contact in the glucagon-GCGR-G_{i1} structure are shown as sticks. The red arrow indicates the movement of Gβ in the G_{i1}-bound structure relative to the G_s-bound structure. (**F** and **G**) Glucagon-induced G_s and G_{i1} activation assays using NanoBiT. (F) G_s activation; (G) G_{i1} activation. Bars represent differences in calculated glucagon potency (pEC_{50}) for each mutant relative to the wild-type receptor (WT). Data are colored according to the extent of effect (yellow, factor of 3 to 5 reduction of EC_{50}; gold, factor of 5 to 10 reduction of EC_{50}; orange, factor of 10 to 30 reduction of EC_{50}). Data are means ± SEM from at least three independent experiments performed in technical triplicate; nd, not determined. *P < 0.05 [one-way analysis of variance (ANOVA) followed by Dunnett's posttest, compared with the response of WT]. See table S2 for detailed statistical evaluation and expression level.

introducing an additional interaction interface between GCGR and G_i mediated by the first intracellular loop (ICL1) of the receptor and Gβ (Fig. 3E and fig. S7, E and K). This binding interface was supported by our mutagenesis studies showing that the K168A mutation abolished G_{i1} activation but had no effect on G_s activation (Fig. 3, F and G; fig. S8, A and D; and table S2). Taken together, the G protein–bound GCGR structures demonstrate that individual intracellular loops play different roles in governing G protein recognition and specificity.

Recognition patterns for the C-terminal α5 helix of $G\alpha_s$ and $G\alpha_{i1}$

Despite the overall similarity in the backbone of the intracellular binding cavity, the two GCGR complex structures exhibit different molecular details in the recognition patterns for the C termini of $G\alpha_s$ and $G\alpha_{i1}$, whereby $G\alpha_{i1}$ forms more limited interactions that are largely hydrophobic and $G\alpha_s$ forms more extensive interactions, both polar and hydrophobic (Fig. 4, A to D, and fig. S7). Two highly conserved class B GPCR polar networks, the HETX motif ($H^{2.50b}$, $E^{3.50b}$, $T^{6.42b}$, and $Y^{7.57b}$) and the helix II-VI-VII-VIII network ($R^{2.46b}$, $R/K^{6.37b}$, $N^{7.61b}$, and $E^{8.41b}$), at the intracellular face of the receptor have been suggested to play critical roles in modulating conformational change upon receptor activation (*10*, *37*). In the G_s-bound GCGR structure, the bulky residue $Y391^{G.H5.23}$ at the α5 helix C terminus binds to a subpocket formed by $R173^{2.46b}$, $H177^{2.50b}$, $E245^{3.50b}$, $Y248^{3.53b}$, $L249^{3.54b}$, and $Y400^{7.57b}$ in GCGR (Fig. 4A). In contrast, the residue at position G.H5.23 is a cysteine ($C351^{G.H5.23}$) in $G\alpha_i$. Without the bulky side chain, this residue only forms weak hydrophobic contacts with $R173^{2.46b}$ and $L249^{3.54b}$ in GCGR (Fig. 4B). Despite the different interaction modes, the mutations $R173^{2.46b}$A, $H177^{2.50b}$A, $E245^{3.50b}$A, and $Y400^{7.57b}$A all impaired glucagon-induced cAMP production and glucagon-induced inositol phosphate (IP) accumulation using a chimeric Gα protein, $G\alpha_{qi9}$ (*32*, *38*) (Fig. 4, E to H; fig. S8, G and J; and tables S3 and S4). This latter assay allowed a cAMP-independent interrogation of the effect of mutants on the C-terminal nine amino acids of $G\alpha_i$ that constitute most of the interaction surface in the G_i complex structure (Fig. 4, B

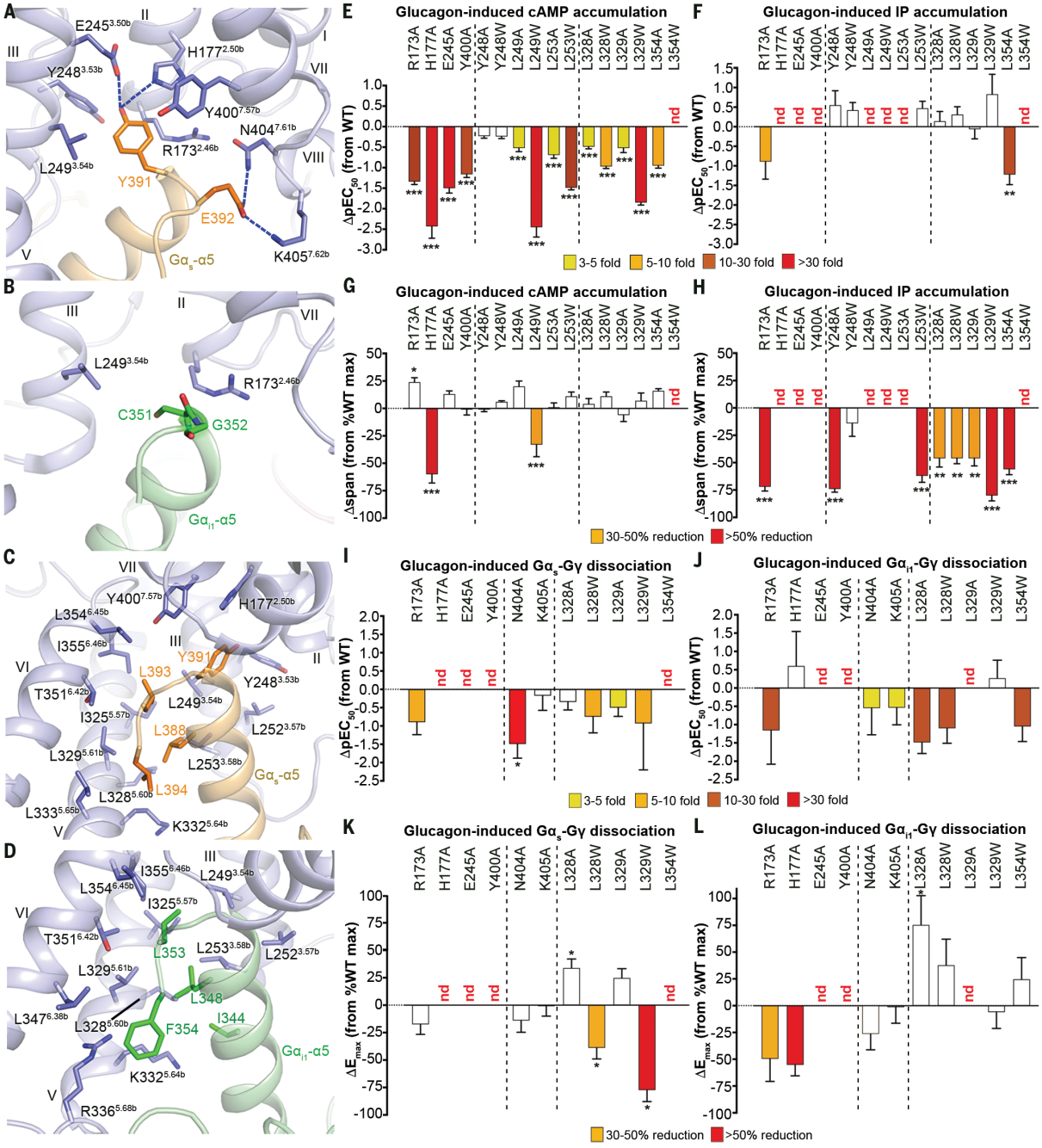

Fig. 4. Interaction patterns for the α5 helix of $G\alpha_s$ and $G\alpha_{i1}$. (**A**) Interactions between GCGR and the $G\alpha_s$ residues $Y391^{G.H5.23}$ and $E392^{G.H5.24}$. The glucagon-GCGR-G_s structure is colored light blue (GCGR) and gold ($G\alpha_s$). The residues involved in interactions are shown as sticks and are colored blue (GCGR) and orange ($G\alpha_s$). Polar interactions are shown as blue dashed lines. (**B**) Interactions between GCGR and the $G\alpha_i$ residues $C351^{G.H5.23}$ and $G352^{G.H5.24}$, showing the limited contact between GCGR and these two residues. The glucagon-GCGR-G_{i1} structure is colored light blue (GCGR) and green ($G\alpha_{i1}$). The residues involved in interactions are shown as sticks and are colored blue (GCGR) and green ($G\alpha_{i1}$). (**C**) Hydrophobic interactions between GCGR and the hydrophobic patch at the C terminus of α5 in $G\alpha_s$. (**D**) Hydrophobic interactions between GCGR and the hydrophobic patch at the C terminus of α5 in $G\alpha_{i1}$. (**E** and **G**) Glucagon-induced cAMP accumulation assay. Bars represent differences in calculated glucagon potency [pEC_{50}, (E)] or maximum glucagon response [span, (G)] for each mutant relative to the wild-type receptor (WT). Data are colored according to the extent of effect. Data are means ± SEM from at least three independent experiments performed in technical triplicate; nd, not determined. *P < 0.01, **P < 0.001, ***P < 0.0001 (one-way ANOVA followed by Dunnett's posttest, compared with the response of WT). See table S3 for detailed statistical evaluation and receptor expression levels. (**F** and **H**) Glucagon-induced IP accumulation assay using the chimeric Gα protein $G\alpha_{qi9}$. Bars represent differences in calculated pEC_{50} (F) or span (H) for each mutant relative to WT. See table S4 for detailed statistical evaluation and receptor expression levels. (**I** and **K**) Glucagon-induced G_s activation assay using NanoBiT. Bars represent differences in calculated glucagon potency [pEC_{50}, (I)] or maximum glucagon response [E_{max}, (K)] for each mutant relative to WT. *P < 0.05 (one-way ANOVA followed by Dunnett's posttest, compared with the response of WT). See table S2 for detailed statistical evaluation and receptor expression levels. (**J** and **L**) Glucagon-induced G_{i1} activation assay using NanoBiT. Bars represent differences in pEC_{50} (J) or E_{max} (L) for each mutant relative to WT. See table S2 for detailed statistical evaluation and receptor expression levels.

and D, and fig. S1E). Additionally, the NanoBiT assay revealed that these alanine replacements heavily impaired both G_s and G_{i1} activation (Fig. 4, I to L; fig. S8, B and E; and table S2). The effect of these mutations on G_s and G_i activation could be explained by the disruption of the interaction networks within the receptor and impairment of the global conformational rearrangement that is required for G protein recognition and signaling. Nonetheless, in the NanoBiT G protein activation assay, there was a greater impact of the H177$^{2.50b}$A mutant on G_s than on G_{i1} (Fig. 4, I to L, and fig. S8, B and E), which may reflect the additional loss of direct interaction that occurs with $G\alpha_s$ Y391$^{G.H5.23}$.

The interaction patterns of GCGR with G_s and G_i also differ for the residue at position G.H5.24 of the Gα α5 helix. The side chain of the $G\alpha_s$ residue E392$^{G.H5.24}$ is within interaction distance of N404$^{7.61b}$ and K405$^{7.62b}$ at the hinge region between helices VII and VIII in the glucagon-GCGR-G_s structure (Fig. 4A and fig. S7B), whereas these interactions are not possible in the G_i complex because of glycine (G352$^{G.H5.24}$) substitution in $G\alpha_i$ (Fig. 4B and fig. S7H). In the NanoBiT assay, a factor of 31 reduction of the EC_{50} in glucagon-induced G_s activation occurred for the mutant N404$^{7.61b}$A, which in contrast had little effect on G_i activation (factor of 4 reduction) (Fig. 4, I and J; fig. S8, B and E; and table S2). However, the mutant K405$^{7.62b}$A was not different from the wild-type GCGR for either G protein, which suggests that interaction with the side chain of this residue is less critical for engagement with G_s.

In both G_s- and G_{i1}-bound GCGR structures, a G protein–binding cavity formed by a cluster of hydrophobic residues from helices III, V, and VI is observed at the intracellular face of the receptor transmembrane domain. It recognizes different hydrophobic patches at the α5 C terminus in $G\alpha_s$ and $G\alpha_i$ ($G\alpha_s$: L388$^{G.H5.20}$, Y391$^{G.H5.23}$, L393$^{G.H5.25}$, and L394$^{G.H5.26}$; $G\alpha_i$: I344$^{G.H5.16}$, L348$^{G.H5.20}$, L353$^{G.H5.25}$, and F354$^{G.H5.26}$) (Fig. 4, C and D). The importance of this hydrophobic cavity in receptor signaling was reflected in our mutagenesis studies, where introduction of alanine or tryptophan mutation within the cavity not only decreased glucagon potency on G_s signaling (Fig. 4, E and G; fig. S8, H and I; and table S3) but also reduced G_{qi9}-mediated IP production (Fig. 4, F and H; fig. S8, K and L; and table S4). Of note, tryptophan mutations within this pocket were more detrimental for G_s signaling than were alanine mutations (Fig. 4E and fig. S8, H and I); this was not the case for G_i, where some tryptophan mutations such as Y248$^{3.53b}$W and L328$^{5.60b}$W were better tolerated than alanine (Fig. 4, F and H, and fig. S8, K and L). The distinct effects of the tryptophan mutants on G_s and G_i activation were also observed in the NanoBiT assay, where L328$^{5.60b}$W and L329$^{5.61b}$W exhibited larger effects on G_s activation [factor of 6 to 8 reduction of potency and 40 to 80% reduction in maximal responses (E_{max})] than their alanine replacements (factor of 2 to 3 reduction of potency and no reduction in E_{max}) (Fig. 4, I and K; fig. S8C; and table S2), but again were better tolerated in the assay of G_{i1} activation (Fig. 4, J and L; fig. S8F; and table S2). Consistent with these results, the mutation L354$^{6.45b}$W substantially reduced both glucagon potency and E_{max} in G_s activation, whereas it showed much less influence on G_{i1} activation (factor of 10 reduction of potency and no reduction in E_{max}) (Fig. 4, I to L; fig. S8, C and F; and table S2). Increasing the size of the hydrophobic residues reduces the size of the intracellular pocket, and this is more detrimental to binding of the bulkier and more polar G_s α5 C terminus.

Most of the alanine replacements—Y248$^{3.53b}$A, L249$^{3.54b}$A, L253$^{3.58b}$A, L328$^{5.60b}$A, L329$^{5.61b}$A, and L354$^{6.45b}$A—reduced the maximum level of G_{qi9}-mediated IP production by 50 to 90% (Fig. 4H, fig. S8K, and table S4). These alanine mutants retained E_{max} values in cAMP accumulation that were similar to that of the wild-type receptor, but decreased potency of glucagon was observed (by a factor of 2 to 9) (Fig. 4, E and G; fig. S8H; and table S3). Although some of these alanine mutants had a similar overall effect on G_s and G_i signaling, Y248$^{3.53b}$A, L249$^{3.54b}$A, L253$^{3.58b}$A, and L354$^{6.45b}$A were more detrimental for G_i signaling (Fig. 4, E to H, and tables S3 and S4). Similarly, in the NanoBiT assay, the mutations L328$^{5.60b}$A and L329$^{5.61b}$A reduced glucagon potency by a factor of >30 in G_{i1} activation but decreased the potency of G_s activation by only a factor of 2 to 3 (Fig. 4, I and J; fig. S8, C and F; and table S2). The different behaviors of these mutants indicate that disturbing the hydrophobic contact between the receptor and the Gα α5 C terminus has a larger effect on G_i signaling than on G_s signaling. This aligns well with the fact that the interaction interface between GCGR and the Gα C terminus (residues G.H5.16 to G.H5.26), which is mainly composed of hydrophobic residues, accounts for 80% of the GCGR-$G\alpha_i$ interface but only about 60% of the total interface between GCGR and $G\alpha_s$. Thus, the hydrophobic cavity within the receptor intracellular face may play a more critical role for G_i recognition than that of G_s.

Collectively, this work provides a model for the diverse G protein signaling observed with class B GPCRs. The G protein–bound GCGR structures reveal that the less bulky G_i protein is accommodated in the large intracellular cavity but forms less extensive, predominantly hydrophobic, interactions, which account for G protein coupling specificity. Furthermore, there are specific conformational differences in the receptor, which also govern the nature of GCGR–G protein interactions and may mediate biased agonism, including in the intracellular loops and individual residue side chains. Although there are studies that implicate G_i coupling of GCGR, physiological relevance remains unclear. Nonetheless, our structures of G_s and G_i bound to the same GPCR give an opportunity to study the basis of G protein specificity and offer new insights into the molecular details that govern pleiotropic GPCR–G protein coupling.

REFERENCES AND NOTES

1. A. J. Venkatakrishnan *et al.*, *Nature* **494**, 185–194 (2013).
2. D. Wootten, L. J. Miller, C. Koole, A. Christopoulos, P. M. Sexton, *Chem. Rev.* **117**, 111–138 (2017).
3. J. Van Rampelbergh *et al.*, *Biochim. Biophys. Acta* **1357**, 249–255 (1997).
4. T. Blank *et al.*, *J. Neurosci.* **23**, 700–707 (2003).
5. D. K. Grammatopoulos, H. S. Randeva, M. A. Levine, K. A. Kanellopoulou, E. W. Hillhouse, *J. Neurochem.* **76**, 509–519 (2001).
6. K. J. Culhane, Y. Liu, Y. Cai, E. C. Yan, *Front. Pharmacol.* **6**, 264 (2015).
7. K. E. Mayo *et al.*, *Pharmacol. Rev.* **55**, 167–194 (2003).
8. Y. L. Liang *et al.*, *Nature* **546**, 118–123 (2017).
9. Y. Zhang *et al.*, *Nature* **546**, 248–253 (2017).
10. Y. L. Liang *et al.*, *Nature* **555**, 121–125 (2018).
11. Y. L. Liang *et al.*, *Nature* **561**, 492–497 (2018).
12. L. H. Zhao *et al.*, *Science* **364**, 148–153 (2019).
13. K. M. Habegger *et al.*, *Nat. Rev. Endocrinol.* **6**, 689–697 (2010).
14. Y. Xu, X. Xie, *J. Recept. Signal Transduct. Res.* **29**, 318–325 (2009).
15. T. Grady, M. Fickova, H. S. Tager, D. Trivedi, V. J. Hruby, *J. Biol. Chem.* **262**, 15514–15520 (1987).
16. E. C. Aromataris, M. L. Roberts, G. J. Barritt, G. Y. Rychkov, *J. Physiol.* **573**, 611–625 (2006).
17. L. H. Hansen *et al.*, *Am. J. Physiol.* **274**, C1552–C1562 (1998).
18. J. D. Kilts *et al.*, *Circ. Res.* **87**, 705–709 (2000).
19. M. Rossi *et al.*, *J. Clin. Invest.* **128**, 746–759 (2018).
20. J. I. Bagger, F. K. Knop, J. J. Holst, T. Vilsbøll, *Diabetes Obes. Metab.* **13**, 965–971 (2011).
21. D. Wootten, J. Simms, L. J. Miller, A. Christopoulos, P. M. Sexton, *Proc. Natl. Acad. Sci. U.S.A.* **110**, 5211–5216 (2013).
22. See supplementary materials.
23. H. Zhang *et al.*, *Nature* **553**, 106–110 (2018).
24. C. J. Draper-Joyce *et al.*, *Nature* **558**, 559–563 (2018).
25. Y. Kang *et al.*, *Nature* **558**, 553–558 (2018).
26. A. Koehl *et al.*, *Nature* **558**, 547–552 (2018).
27. J. García-Nafría, R. Nehmé, P. C. Edwards, C. G. Tate, *Nature* **558**, 620–623 (2018).
28. J. García-Nafría, C. G. Tate, *Mol. Cell. Endocrinol.* **488**, 1–13 (2019).
29. K. Krishna Kumar *et al.*, *Cell* **176**, 448–458.e12 (2019).
30. S. Maeda, Q. Qu, M. J. Robertson, G. Skiniotis, B. K. Kobilka, *Science* **364**, 552–557 (2019).
31. N. Okashah *et al.*, *Proc. Natl. Acad. Sci. U.S.A.* **116**, 12054–12059 (2019).
32. B. R. Conklin, Z. Farfel, K. D. Lustig, D. Julius, H. R. Bourne, *Nature* **363**, 274–276 (1993).
33. T. Flock *et al.*, *Nature* **524**, 173–179 (2015).
34. A. S. Rose *et al.*, *J. Am. Chem. Soc.* **136**, 11244–11247 (2014).
35. A. S. Dixon *et al.*, *ACS Chem. Biol.* **11**, 400–408 (2016).
36. H. E. Kato *et al.*, *Nature* **572**, 80–85 (2019).
37. D. Wootten *et al.*, *Biochem. Pharmacol.* **118**, 68–87 (2016).
38. C. Monnier *et al.*, *EMBO J.* **30**, 32–42 (2011).

ACKNOWLEDGMENTS

We thank Y.-L. Liang for expert advice on class B GPCR–G protein complex biochemistry, and T. T. Truong and S. Darbalaei for assistance with the NanoBiT studies. The cryo-EM studies were performed at the Center for Biological Imaging (CBI, http://cbi.ibp.ac.cn), Institute of Biophysics, Chinese Academy of Sciences; we thank B.-L. Zhu and X. Huang from CBI for their help on cryo-EM data collection. **Funding:** Supported by the National Key R&D Program of China 2018YFA0507000 (B.W., Q.Z., and M.-W.W.) and 2017YFA0504703 (F.S.); National Science Foundation of China grants 31825010 (B.W.), 81525024 (Q.Z.), 31830020 (F.S.), 81872915 (M.-W.W.), and 81773792 (D.Y.); CAS Strategic Priority Research Program XDB37000000 (B.W.); Shanghai Outstanding Academic Leaders Plan of Shanghai Municipal Science and Technology Committee 18XD1404800 (Q.Z. and S.H.); the National Science & Technology Major Project–Key New Drug Creation and Manufacturing Program, China grant 2018ZX09711002 (L.M., D.Y., and M.-W.W.); the National Mega R&D Program for Drug Discovery

grant 2018ZX09735-001 (M.-W.W.); Shanghai Science and Technology Development Fund 16ZR1407100 (A.D.); and Australian National Health and Medical Research Council (NHMRC) grants 1126857 (D.W.) and 1150083 (P.M.S.). D.W. is an NHMRC Senior Research Fellow and P.M.S. is a Senior Principal Research Fellow. **Author contributions:** A.Q. optimized the constructs, developed the expression and purification procedures, and prepared the protein samples for cryo-EM; S.H. helped with protein sample optimization and performed negative-stain EM data acquisition and analysis, cryo-EM data processing and analysis, model building, and structure refinement; X.L. performed cryo-sample preparation, acquired cryo-EM data, and assisted with data processing and analysis; A.Q. and Z.L. performed signaling assays with assistance from R.C.; P.Z. performed NanoBiT assays; A.D. performed the ligand-binding assay; L.T. performed preliminary cryo-EM screening and assisted with data processing and analysis; Q.T. helped with negative-stain EM data acquisition/analysis and cryo-EM data collection; X.C. and L.M. expressed the proteins; R.C. and T.S.T. helped with protein purification optimization; D.Y. and M.-W.W. oversaw ligand binding studies; P.M.S. and D.W. oversaw the NanoBiT assay; F.S. oversaw EM data acquisition, analysis, and processing; S.R.-R., D.Y., M.-W.W., P.M.S., D.W., and F.S. helped with data analysis/interpretation and edited the manuscript; and B.W. and Q.Z. initiated the project, planned and analyzed experiments, supervised the research, and wrote the manuscript with input from all co-authors. **Competing interests:** S.R.-R. is an employee and stock owner of Novo Nordisk, a pharmaceutical company focused on treatment of diabetes and obesity. All other authors declare no competing interests. **Data and materials availability:** Atomic coordinates and the cryo-EM density maps for the structures of glucagon-GCGR-G_s and glucagon-GCGR-G_{i1} have been deposited in the RCSB Protein Data Bank (PDB) with identification codes 6LMK and 6LML, and the Electron Microscopy Data Bank (EMDB) under accession codes EMD-0917 and EMD-0918. All other data are available in the manuscript or the supplementary materials. Reagents are available from the corresponding authors upon reasonable request.

SUPPLEMENTARY MATERIALS

science.sciencemag.org/content/367/6484/1346/suppl/DC1
Materials and Methods
Supplementary Text
Figs. S1 to S8
Tables S1 to S4
References (*39*–*53*)

17 September 2019; accepted 11 February 2020
10.1126/science.aaz5346

Structural basis of G_S and G_i recognition by the human glucagon receptor

Anna Qiao, Shuo Han, Xinmei Li, Zhixin Li, Peishen Zhao, Antao Dai, Rulve Chang, Linhua Tai, Qiuxiang Tan, Xiaojing Chu, Limin Ma, Thor Seneca Thorsen, Steffen Reedtz-Runge, Dehua Yang, Ming-Wei Wang, Patrick M. Sexton, Denise Wootten, Fei Sun, Qiang Zhao and Beili Wu

Science **367** (6484), 1346-1352.
DOI: 10.1126/science.aaz5346

Choosing a partner that fits

G protein–coupled receptors (GPCRs) are responsible for transducing diverse signals from outside to inside cells. This process requires specificity both in ligand binding to GPCRs and in coupling between GPCRs and their intracellular partners, G proteins. Qiao *et al.* determined the structure of the human glucagon receptor (GCGR), a type B GPCR, bound to glucagon and one of two heterotrimeric G proteins, G_s or G_{i1}. GCGR signals mainly through G_S, and the structures provide a basis for this specificity. Conformational changes in GCGR, relative to the inactive state, create a binding cavity for the G proteins. The pocket is opened sufficiently to accommodate a bulky binding motif in G_S. G_{i1} can still bind but the pocket does not close around it, so there is a smaller interaction interface.

Science, this issue p. 1346